

Research Article

Delamination Localization in Sandwich Skin Using Lamb Waves by Finite Element Method

Salah Nissabouri ¹, Mhammed El allami,^{1,2} El Hassan Boutyour,¹ and Ahmed Errkik¹

¹LMEET Lab, Department of Applied Physics, FST, Settat 26000, Morocco

²CRMEF, Settat, Morocco

Correspondence should be addressed to Salah Nissabouri; s.nissabouri@uhp.ac.ma

Received 15 June 2018; Revised 13 October 2018; Accepted 12 November 2018; Published 28 November 2018

Academic Editor: Kim M. Liew

Copyright © 2018 Salah Nissabouri et al. This is an open access article distributed under the Creative Commons Attribution License, which permits unrestricted use, distribution, and reproduction in any medium, provided the original work is properly cited.

In this work we model by finite element method (FEM) the Lamb waves' propagation and their interactions with symmetric and asymmetric delamination in sandwich skin. The simulations were carried out using ABAQUS CAE by exciting the fundamental A_0 Lamb mode in the frequency 300 kHz. The delamination was then estimated by analysing the signal picked up at two sensors using two technics: Two-Dimensional Fast Fourier Transform (2D-FFT) to identify the propagating and converted modes, and wavelet transform (WT) to measure the arrival times. The results showed that the mode A_0 is sensible to symmetric and asymmetric delamination. Besides, based on signal changes with the delamination edges, a localization method is proposed to estimate the position and the length of the delamination. In the last section an experimental FEM verification is provided to validate the proposed method.

1. Introduction

A sandwich composite is a material made from two thin skins bonded to a thick core. The skin studied in this paper is an orthotropic plate $[0]_4$ with three mutually perpendicular planes of symmetry. The sandwich materials are designed to improve mechanical properties of structures. They are widely used in different fields especially in aeronautic industry. Their properties are influenced by the proportions of the matrix and the reinforcements. There are other parameters that also affect their characteristics like size, orientation, and distribution of the fibre. However, the heterogeneity of the composites structures leads to their weakness and facilitates the appearance of internal and external damage such as fibre breakage, matrix cracking, through-thickness hole, local delamination. Among these types of damage, delamination is especially easy to appear because the transverse tensile and interlaminar shear strengths are weak compared to the in-plane strength [1]. The delamination causes wave scattering, mode conversion, and multiple reflections. To understand these mechanisms, theoretical, numerical, and experimental studies are conducted.

Feng, Lopes Ribeiro, and Geirinhas Ramos [2] analysed the interaction of symmetric S_0 and antisymmetric A_0 mode with the delamination using finite element simulations. The Lamb waves propagation in a 4-layer $[0/90]_s$ laminate were compared with propagations obtained in 1-layer $[0]$ and in 3-layer $[90/90/0]$ sublaminates. Chiu, Roseb, and Nadarajah [3] investigated the scattering of the S_0 mode by a delamination in quasi-isotropic fibre-composite laminate. Guo and Cawley [4] studied by finite element analysis and by experiment the interaction of the S_0 Lamb mode with delamination. Nadarajah, Vien, and Chiu [5] presented results for the scatter field for various angles of incidence and for varying defect sizes. Hayashi and Kawashima [6] studied the reflections of Lamb waves at a delamination by semianalytical finite element method. Ching-Tai and Veidta [7] investigated the scattering characteristics of A_0 mode Lamb wave at a delamination in a quasi-isotropic composite laminate. Bin [8] suggested an algorithm to localize and identify the damage in Woven Glass Fibre reinforced epoxy (WGF/epoxy). Mustapha [9] characterized fundamental symmetric and antisymmetric Lamb modes in terms of their velocity and magnitude variation as they change gradually in the thickness

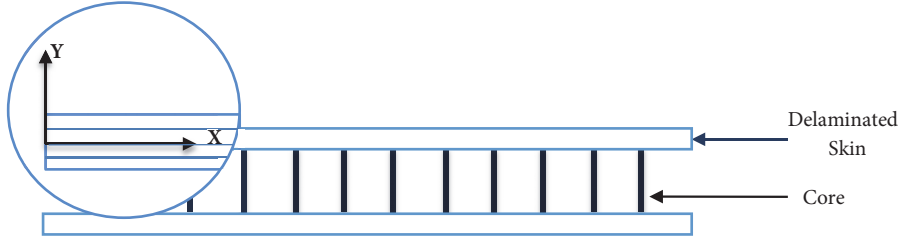


FIGURE 1: Sandwich structure with delaminated skin.

of a composite sandwich plate with a high density foam core. Ng [10] presented a theoretical and finite element (FE) investigation of the scattering characteristics of A_0 at delaminations in a quasi-isotropic composite laminate. Veidt and Ng [11] studied the influence of stacking sequence on fundamental antisymmetric Lamb wave (A_0) scattering characteristics through holes in composite laminates. Luca [12] developed a valid finite element model to simulate Lamb waves' propagation in a Carbon Fibre Reinforced Plastic (CFRP) laminate for damage detection purpose and investigated the effects of the wave interaction with respect to damage parameters such as size and orientation. Yang [13] investigated some aspects of numerical simulation of excitation and detection of Lamb waves using piezoelectric disks in plate-like composite laminates.

In this paper, a numerical approach is proposed to localize a delamination in sandwich skin as presented in Figure 1. The aim of this work is to study the conversion by identifying the propagating modes and also to evaluate the symmetric and asymmetric delamination.

2. Lamb Waves Theory

Lamb waves are most used for many reasons; they can propagate long distances along plates and shells so they permit quick inspection of large structures, and also they are sensitive to the small variations either in material properties or in structure of the plate. However, they are dispersive which means that the interpretation of received signals can be complicated. So the key is to choose one pure mode to excite and to analyse its reflection, conversion, and transmission.

2.1. Equation of Lamb Waves Propagation in Unidirectional Lamina. The characteristic equations of the symmetrical and antisymmetric waves are [14]

$$\begin{aligned} D_{11}D_{23} \cotan\left(\frac{k\alpha_1 h}{2}\right) - D_{13}D_{21} \cotan\left(\frac{k\alpha_3 h}{2}\right) &= 0 \\ D_{11}D_{23} \tan\left(\frac{k\alpha_1 h}{2}\right) - D_{13}D_{21} \tan\left(\frac{k\alpha_3 h}{2}\right) &= 0 \end{aligned} \quad (1)$$

with D_r coefficients calculated by the following equations:

$$\begin{aligned} D_{1r} &= C_{13} + C_{33}\alpha_r W_r \\ D_{2r} &= C_{55}(\alpha_r + W_r) \end{aligned} \quad (2)$$

$W_r = (\rho c^2 - C_{11} - C_{55}\alpha_r^2)/(C_{13} + C_{55})\alpha_r$. For $r \{1, 2, 3, \text{ and } 4\}$, with

$$\begin{aligned} \alpha_1 &= -\alpha_2 = \frac{-B - \sqrt{B^2 - 4AC}}{2A} \\ \alpha_3 &= -\alpha_4 = \frac{-B + \sqrt{B^2 - 4AC}}{2A} \\ \alpha_5 &= -\alpha_6 = \sqrt{\frac{\rho c^2 - C_{66}}{C_{44}}} \end{aligned} \quad (3)$$

coefficients A , B and C are calculated by the following equations:

$$\begin{aligned} A &= C_{33}C_{55} \\ B &= C_{33}(C_{11} - \rho c^2) + C_{55}(C_{55} - \rho c^2) - (C_{13} + C_{55})^2 \\ C &= (C_{11} - \rho c^2)(C_{55} - \rho c^2) \end{aligned} \quad (4)$$

where h is the skin thickness, k is the wavenumber corresponding to the X direction, c is the phase velocity. C_{11} , C_{13} , C_{33} , C_{44} , C_{55} , C_{66} are the elastic constants, and ρ is the skin density.

2.2. Dispersion Curves. The dispersion curves presented in Figure 2 for orthotropic plate $[0]_4$ are plotted using DISPERSE program [15] in terms of wavenumber versus frequency.

At low frequency, two modes, A_0 and S_0 , can propagate. As the frequency increases, more modes are possible to propagate.

2.3. Lamb Waves Control Technics. Among the contact technics to generate and to receive the signal, we find two methods: pitch catch and pulse echo. These two technics are simple but they require the coupling medium which limits the transmission of acoustic power.

In the pulse-echo method, the reflected signal permits evaluating the damage. In the pitch catch technic the transducer placed in the transmission side permits evaluating the defect. In this paper two methods have been used to evaluate the delamination.

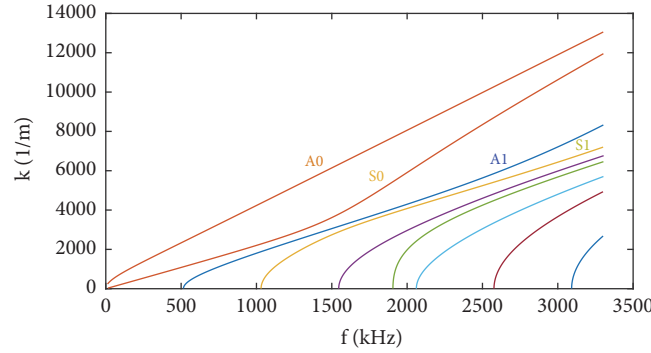


FIGURE 2: Dispersion curves (wavenumber versus frequency).

3. Postprocess Tools

3.1. *2D-FFT Analysis.* Lamb waves' propagation is sinusoidal in the frequency and spatial domains. For that reason, a temporal Fourier Transform is applied to go from the time to frequency domain; after that, a spatial Fourier Transform is computed to obtain the frequency wavenumber domain; see [16]. In practice, carrying out a spatial Fourier method to data obtained experimentally or numerically requires applying a 2D-FFT, using the following.

$$H(k, f) = \iint_{-\infty}^{+\infty} u(x, t) e^{-i(kx+\omega t)} dx dt \quad (5)$$

3.2. *Wavelet Analysis.* Wavelet transform is an important tool in the time frequency domain of transient signals. The continuous wavelet transform of signal $u(t)$ is defined as follows.

$$cwt(a, b) = \frac{1}{\sqrt{|a|}} \int_{-\infty}^{+\infty} u(t) \psi^* \left(\frac{t-b}{a} \right) dt \quad (6)$$

The obtained signal is a function of a and b , the translation and scale parameters, respectively. The parameter $\psi(t)$ is the transforming function named the mother wavelet. In this paper we use wavelet transform by "gaus1" to locate the peak which permits determining the arrival time of the wave at specific frequency. Moreover, for each frequency f , the localization of maximal value of the wavelet coefficients $cwt(a, b)$ allows identifying the arrival times t_1 and t_2 . Knowing the group velocity and the delay ($\Delta t = t_2 - t_1$) between the two modes with the same nature, we can calculate the distance by the following equation.

$$\Delta x = V_g \Delta t \quad (7)$$

Knowing the delay between two different modes (symmetric and antisymmetric), we calculate the distance by the following equation:

$$\Delta x = \Delta V_g \Delta t \quad (8)$$

with

$$\Delta V_g = \frac{V_S V_A}{V_S - V_A}. \quad (9)$$

Here V_S and V_A are the group velocities, respectively, of S_0 and A_0 modes. Arrival time method was used by many authors to localize the delamination; see [17].

4. Numerical Model Using FEM

Numerical simulations were carried out using finite element software ABAQUS to predict the A_0 Lamb wave propagation behaviour in a $[0]_4$ plate. A number of modelling methods had been used by previous researchers to model the propagating wave: finite difference, boundary elements, strip elements, hybrid and finite element. The finite element method has been extensively and successfully used to model the Lamb waves and study their interactions with defects in structures [18]. Many researchers have used the numerical simulation to study Lamb waves. Chiu, Roseb, and Nadarajah [3] built a 3D model in ABAQUS of the 8-ply laminate $[45/-45/0/90]_S$. Guo and Cawley [4] investigated the influence of delamination position through the thickness and its interaction with the S_0 mode using finite element analysis. The composite laminate modelled was the eight-layer cross-ply. Nadarajah, Vien, and Chiu [5] studied the scattering of a zero-order antisymmetric (A_0) Lamb wave mode by semicircular mid-plane edge delamination using the commercial FE package ABAQUS. Hayashi and Kawashima [6] studied Lamb waves' propagation in laminated plates with delamination using the Strip Element Method and discussed the reflection and transmission for the case S_0 and A_0 excitation. Ng [10] modelled the delamination as a volume split in quasi-isotropic plate. The FE results were carried out by the explicit FE code LS-DYNA. Ng and Veidta [7] used a three-dimensional FE method to simulate an eight-ply $[45/-45/0/90]_S$ quasi-isotropic composite laminate with a delamination. The simulations were computed by ANSYS software. Panda [19] presented 3D FE simulations that were carried out to visualize the wave propagation and their interaction with the defect at various depths of an 8-layered Glass Fibre Reinforced Polymer (GFRP) by finite element software ABAQUS/Explicit. Ramadas [20] investigated the interaction of the primary antisymmetric mode A_0 with symmetric delamination type defects in a quasi-isotropic laminated composite using 2D model ANSYS. Soleimanpour and Ng [21] used 3D explicit finite element method to study cross-ply

TABLE I: Elastic coefficients C_{ij} and density ρ of the material.

ρ (kg/m ³)	C_{11} (GPa)	$C_{22} = C_{33}$	$C_{12} = C_{13} = C_{23}$	$C_{55} = C_{66}$
1530	56,9	14,7	9,76	4,16

laminated composite beams $[0/90/0/90]_S$; they investigated the mode conversion and scattering characteristics of guided waves at delamination. Gudimetla and Kharidi [22] showed a procedure to simulate the propagation of Lamb waves in 8-layered Carbon Reinforced Fibre Plastic (CRFP) using a 2D model in ANSYS. The authors simulate the propagating Lamb waves along the plane of the structure in the form of a time dependent force excitation. Basri and Chiu [18] investigated how Lamb waves respond to the presence of material degradation in a plate-like structure using a series of finite element analyses. The propagation of these guided waves was interpreted with the dispersion characteristics, and displacement profiles were analysed in the frequency and wavenumber domain.

In this paper we try to predict the interaction of A_0 mode in orthotropic plate. The 2D numerical simulations were carried out using ABAQUS CAE. We consider the Lamb waves propagation only in the skin to simplify the propagating modes identification. This assumption has been made in many papers [23–25]. They consider only the propagation in skin as its acoustic impedance is more than the acoustic impedance of the core.

The skin has a length of $L=400$ mm and a thickness of $h = 1.6$ mm. The mechanical properties of each lamina are shown in Table I. Once the geometry of the plate has been achieved, it remains to mesh and to define a sampling sufficient time.

4.1. Meshing and Time Sampling. To satisfy an accurate solution, the model has been meshed using (10), and the time step is calculated by (11).

$$\max(\Delta x, \Delta y) < \frac{\lambda_{min}}{10} \quad (10)$$

$$\Delta t < 0.7 \frac{\max(\Delta x, \Delta y)}{V_L} \quad (11)$$

4.2. Excitation. In order to identify accurately the propagating modes, the simulation is performed on the range of frequencies to prevent dispersive phenomenon. For that reason we choose 300 kHz as frequency of excitation (see Figure 3).

5. Localization Method

The finite element method with ABAQUS CAE code is used to compute the temporal displacement by 2D-FFT technic (5) so as to identify the propagating and converted modes. Once the modes are identified, the next step consists in calculating the arrival times by WT (6). So there are two cases: in the first case, where there is no modes conversion, the time delay permits calculating the delamination position by (7); in the

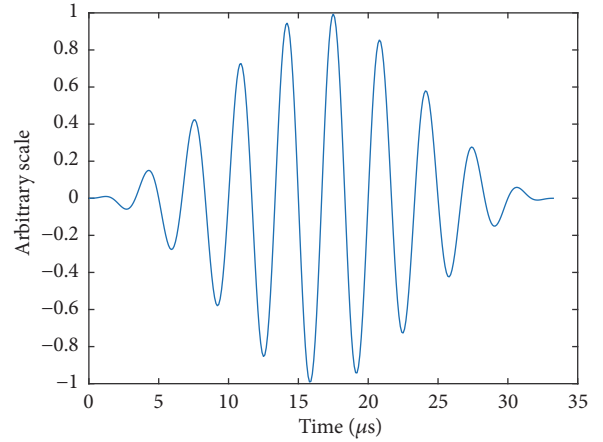


FIGURE 3: Excitation windowed by Hann window.

second case, where the mode converts to another (A_0 to S_0 or S_0 to A_0), (8) is used.

6. Results and Discussion

6.1. Model: $[0]_4$ without Defect. The A_0 mode was excited from the left edge of the plate by concentrated force at the actuator C (see Figure 4). The A_0 Lamb wave is the focus in this study because of its sensitivity to the small defects. To verify the excitability of pure mode A_0 , 2D-FFT was performed at the sensor A. A matrix was calculated at uniformly spaced points.

Figure 5 shows that there is only one mode propagating which is A_0 .

6.2. Model: Symmetric Delamination 60×0.1 . Figure 6 is the delaminated model. Figure 7 is a snapshot of FE out-of-plane displacement. The Lamb waves split into two parts and travel independently with different velocities in the upper and the lower sublaminates. Mode conversions happen at the two edges of a delamination due to the change of boundary conditions. To characterize the delamination, we analysed the signals picked up at the sensors A and B.

6.3. Modes Conversion. In Figure 8, the first wave group is a forward traveling wave group, which is an excited A_0 mode at $x = 0$. When this interacted with the entrance of the delamination, there was a low amplitude reflected wave group. This reflected wave group appears as the second wave group A_0A_0 . Delamination separates the plate into two sublaminates: upper and lower. The transmitted wave converted to the symmetric and antisymmetric mode A_0S_0 and A_0A_0 which traveled within the sublaminates with different velocities. The first wave A_0S_{0U} —U, L mean that the mode travel,

TABLE 2: Delamination localisation from data acquired at sensor A.

Delamination Position	Length	P_D	P_{DTH}	Error %	L_D	Error %
1 and 2	60	103,8	100	3,8	62,0	3,3
	90	103,9	100	3,9	93,3	3,7
	120	103,8	100	3,8	123,4	2,9
2 and 3	60	103,2	100	3,2	62,2	3,7
	90	106,6	100	6,6	94,1	4,5
	120	103,1	100	3,1	120,9	0,8

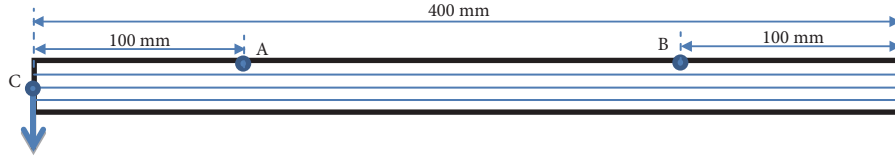


FIGURE 4: Numerical model without defect, C: actuator, A and B: sensors.

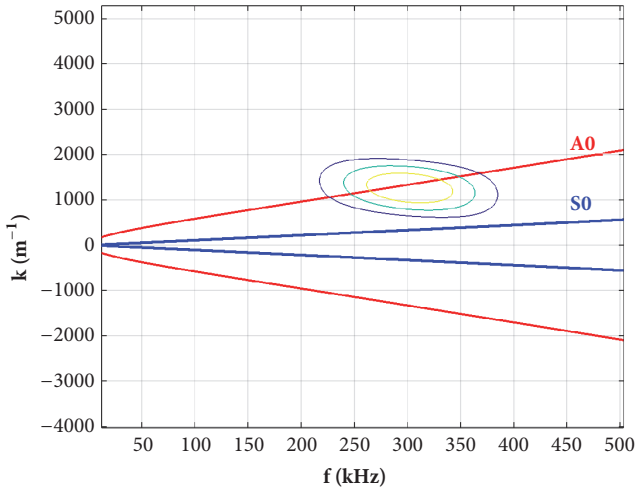


FIGURE 5: Superposition of 2D-FFT over analytical dispersion curves.

respectively, in the upper and lower sublaminates—reached first the exit of delamination; this is justified by the fact that symmetric mode is faster than the antisymmetric mode. The backward mode $A_0S_{0U}S_{0U}$ passes through the upper and then is transmitted to the main laminate as the second wave group $A_0S_{0U}S_{0U}A_0$. By the same manner, in the lower sublaminates the mode $A_0S_{0L}S_{0L}$ is transmitted to the main laminate as $A_0S_{0L}S_{0L}A_0$. In the case of symmetric delamination the two modes $A_0S_{0U}S_{0U}A_0$ and $A_0S_{0L}S_{0L}A_0$ are reflected at the same time.

6.4. Results: Sensor A. Figure 9 is A-scan image from the numerical simulations, taken at 100 mm for a delamination length of 60 mm. As explained in Figure 8, we conclude that the first arrived wave is the incident mode A_0 and the second is the first reflected wave A_0A_0 . The delamination is symmetric so two waves arrived at the same time as one packet which is $A_0S_{0U}S_{0U}A_0 + A_0S_{0L}S_{0L}A_0$.

Based on the 2D-FFT computed using Matlab program applied to the surface of delaminated skin (before the delamination), Figure 10 shows that the incident and the reflected modes are antisymmetric which confirms that the first reflected mode is A_0A_0 .

6.5. Characterization of Delamination from Data Acquired at Sensor A. Figure 11 presents wavelet coefficients versus time at sensor A. The time delay between the peaks permits estimating the position and the length of delamination.

Knowing the group velocity of the modes A_0 and S_0 : $V_g(A_0, 300\text{kHz}) = 1268 \text{ m/s}$, $V_g(S_0, 300\text{kHz}) = 5649 \text{ m/s}$, we can calculate the delamination position from the sensor A noted P_D by Δt_1 (Delta 1) and delamination length noted L_D by Δt_2 (Delta 2) as presented in Table 2.

The sensor A permits evaluating the position and the length of symmetric and asymmetric delamination. The errors associated with the predicted symmetric delamination position range from 3.1% to 6.6%. However in the case of asymmetric delamination, the error is less than 3.8%. As far as the length prediction is concerned, the errors range from 3.6% to 6.9% in symmetric delamination and from 2.9% to 5.9% in asymmetric delamination. So we conclude that the longer the delamination, the higher the estimation.

6.6. Results: Sensor B. Figure 12 represents different wave modes in the case where A_0 mode is incident on the transmission side of the main laminate at sensor B.

This figure represents different wave modes in the case where A_0 mode is incident on the transmission side of the main laminate at sensor B. A new mode S_0 was generated when the A_0 interacted with the entrance of delamination as shown in Figure 8. This new mode traveled within the upper sublaminates along the length of delamination. Then it reached the exit of delamination, interacted with the exit, and generated a new mode A_0 in the forward direction. This new mode propagated in the main laminate, called the $A_0S_{0U}A_0$ mode. In the lower sublaminates the mode is called $A_0S_{0L}A_0$.

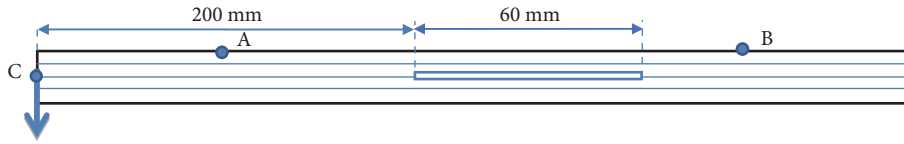


FIGURE 6: Numerical model of symmetric delamination.

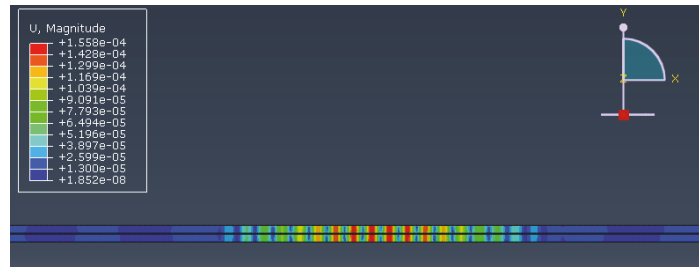


FIGURE 7: Snapshot of FE simulated out-of-plane displacement in the upper and the lower sublaminates separated by the delamination.

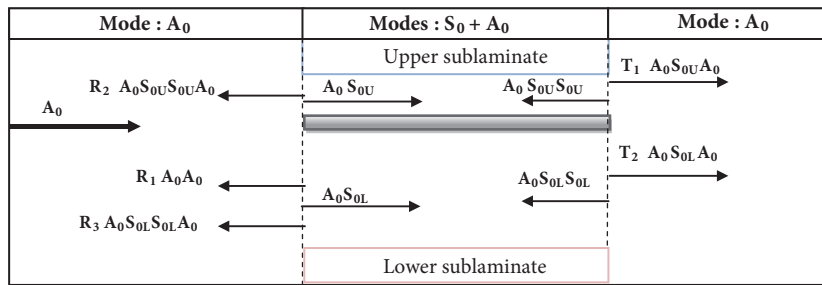


FIGURE 8: A_0 reflection at the entrance and at the end of asymmetric delamination (length 60), case A_0 incident; R denotes reflected mode and T denotes transmitted mode.

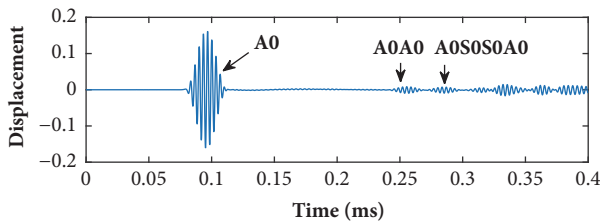


FIGURE 9: Out-of-plane displacement, taken on damaged composite $[0]_4$ at $x = 100$ mm, case symmetric delamination length 60.

Two modes arrived at the same time in the case of symmetric delamination.

6.7. Characterization of Delamination from Data Acquired at Sensor B. Figure 13 presents wavelet coefficients versus time at sensor B. The Δt_1 is the time delay between two transmitted symmetric modes. The Δt_2 is the time delay between the first transmitted symmetric mode and the third antisymmetric mode, so knowing the group velocity of the mode S_0 : $V_g(S_0, 300 \text{ kHz}) \approx 5649 \text{ m/s}$, we can calculate the delamination length noted L_{D1} by (7) and L_{D2} by (8). Table 3 resumes the results found.

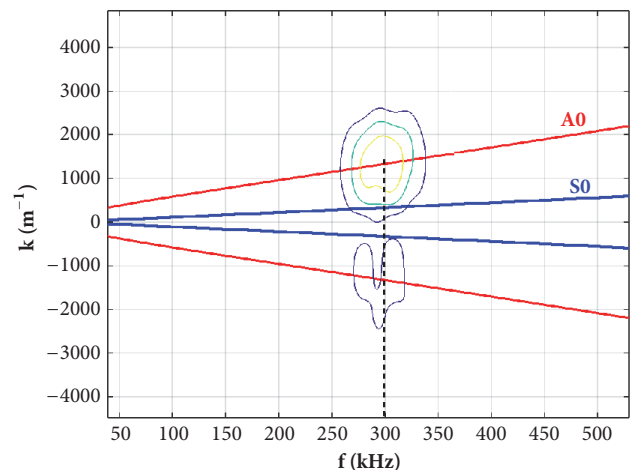


FIGURE 10: Superposition of 2D-FFT applied before the delamination over analytical dispersion curves.

The sensor B permits evaluating only the length of symmetric and asymmetric delamination. The errors associated with the predicted symmetric delamination length range from 1.2% to 4.9%. In the case of asymmetric delamination

TABLE 3: Delamination localisation from data acquired at sensor B.

Delamination Position	Length	L_{D1}	Error %	L_{D2}	Error %	Min Error %
1 and 2	60	49,1	18,1	62,1	3,5	3,5
	90	93,5	3,9	95,2	5,7	3,9
	120	127,1	5,9	127,7	6,4	5,9
2 and 3	60	45,5	24,2	62,9	4,9	4,9
	90	98,9	9,8	94,0	4,5	4,5
	120	121,5	1,2	122,5	2,1	1,2

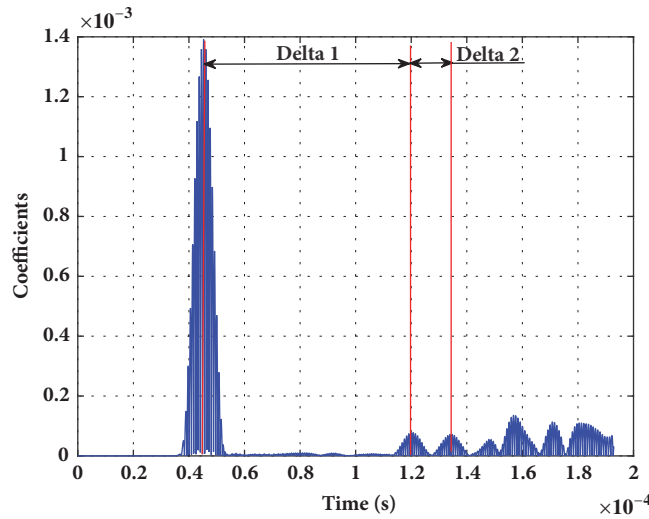


FIGURE 11: Coefficients of wavelet gauss1, case A_0 incident, delamination length 60, between layer 2 and layer 3.

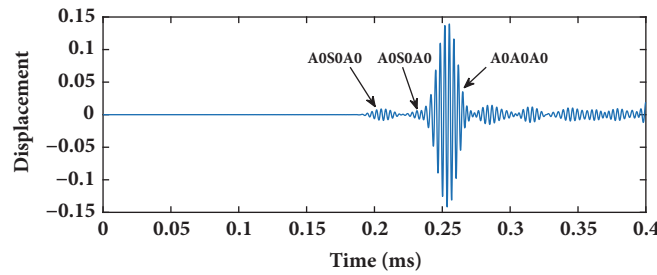


FIGURE 12: Out-of-plane displacement, taken on damaged composite $[0]_4$ at $x = 300$ mm, case symmetric delamination length 60.

the errors range from 3.5% to 5.9%. So we conclude that the longer the delamination, the higher the estimation. Also, the sensor B gives accurate estimation in case of symmetric delamination.

7. Experimental Verification

We validate our model based on Barra results [23]; the author studied by FEM the A_0 Lamb mode interaction with delamination in sandwich skin. Based on Fourier Diamond [26, 27], he has estimated the delamination length. The obtained results are validated by experimental study. These studies have been done by the propagation of Lamb waves on air by using a Laser Doppler velocimetry.

To validate our model and our method we followed the same methodology, as presented in Figure 14.

The $S(x, t)$ is the measured time-displacement matrix at the skin surface. IFFT is the Inverse Fast Fourier Transform.

7.1. Model: Delamination 24×0.1 . The B-scan illustrated in Figure 16 represents the $S(x, t)$: time-displacements matrix picked up at the surface of limited zone (see Figure 15).

Figure 16(a) indicates all the interactions of A_0 Lamb mode with delamination in the skin. Figure 16(b) is the temporal evolution of out-of-plane displacement on the upper surface at $x = 185$ mm (blue line). To evaluate the defect length, and following the Diamond method, we have first of all separated the incident and the reflected waves.

TABLE 4: Comparison between results at sensors A and B.

Delamination Position	Length	Sensor A		Sensor B	
		L_D	Error %	L_D	Error %
1 and 2	60	62,0	3,3	62,1	3,5
	90	93,3	3,7	93,5	3,9
	120	123,4	2,9	127,1	5,9
2 and 3	60	62,2	3,7	62,9	4,9
	90	94,1	4,5	94,0	4,5
	120	120,9	0,8	121,5	1,2
3 and 4	60	62,0	3,3	62,1	3,5
	90	93,3	3,7	93,5	3,9
	120	123,4	2,9	127,1	5,9

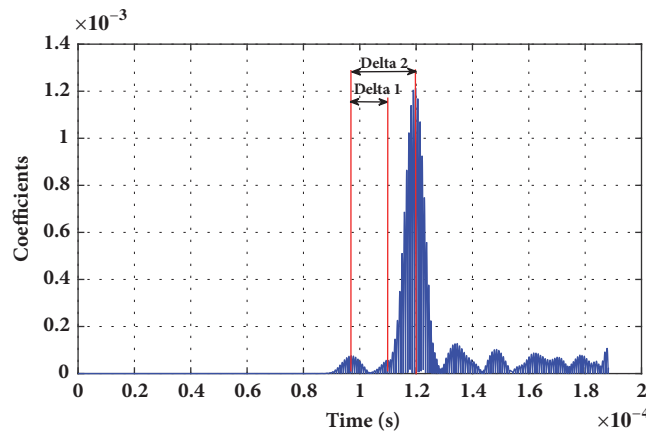


FIGURE 13: Coefficients of wavelet gaus1, case symmetric delamination length 60.

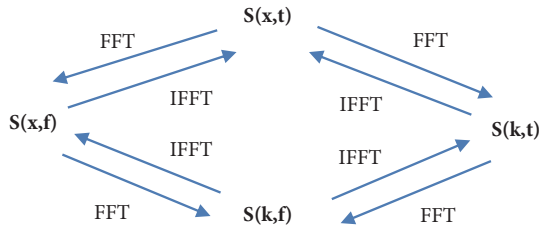


FIGURE 14: Fourier Diamond.

Then the separated incident waves get filtered to remove the undesirable reflections.

Figure 17 shows the filtered incident waves. We can easily see the mode perturbation in the studied zone. This is due to the delamination presence. To evaluate the defect length we computed the temporal FFT to the filtered signal as presented in Figure 18.

Figure 18 shows the principal lobe localized at the frequency 300 kHz which verifies the excitation frequency. To measure the delamination length, a cut of the temporal FFT at the frequency 300 kHz must be done to show clearly the peaks of the lobes.

Figure 19 permits measuring the delamination length. We measure it between the peaks of the lobes. The delamination length is 22 mm.

To conclude, the model gives an accurate result with an error of 8.3%. The errors are due to the approximated numerical model.

8. Conclusions

In this work, we have studied the numerical model describing the propagation of antisymmetric mode A_0 within a sandwich skin. Simulations based on finite element method were carried out using ABAQUS software in order to investigate the interaction of Lamb wave mode by symmetric and asymmetric through-thickness delamination. The results showed the conversion phenomenon. To quantify the conversion and to characterize the delamination, we have computed the 2D-FFT in order to identify the propagating and the converted modes; after that, the WT was calculated at sensors A and B to measure the arrival times.

Table 4 compared the delamination length calculated at the two sensors A and B. It shows that sensor A gives more accurate estimation than sensor B. Moreover, sensor A permits also estimating the start of the delamination. So the optimal position to evaluate the position and the length of delamination is between the actuator and the defect.

Moreover, comparing the signals obtained at two sensors: A and B, it was found that the mode conversions happen at the edges of a delamination for A_0 wave. In fact, this mode

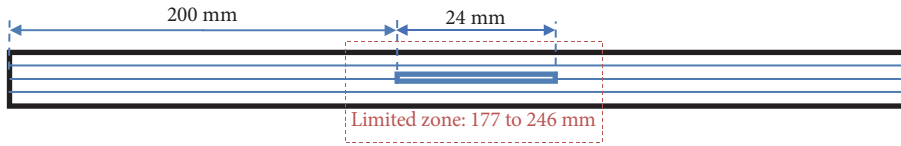


FIGURE 15: Model geometry.

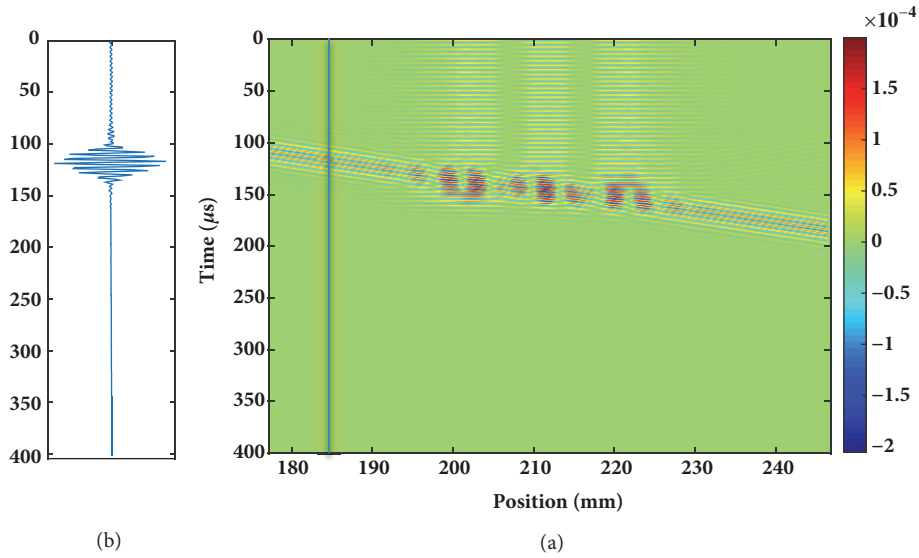


FIGURE 16: (a) Wavefields of A_0 mode interaction with delamination. (b) Cut of $S(x, t)$ at the position 185 mm.

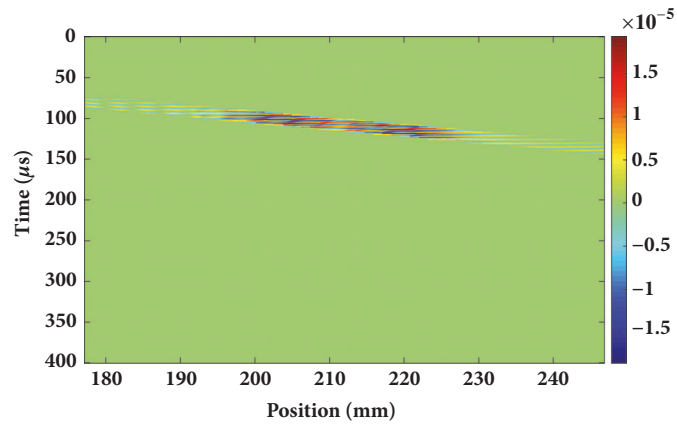


FIGURE 17: Filtered wavefields of incident waves.

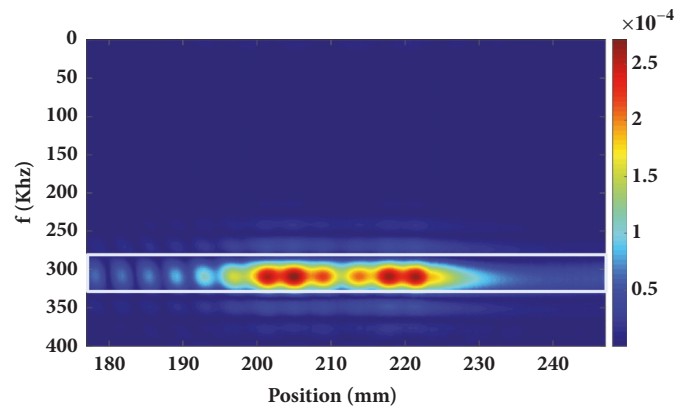


FIGURE 18: $S(x, f)$ temporal FFT applied to the filtered incident waves.

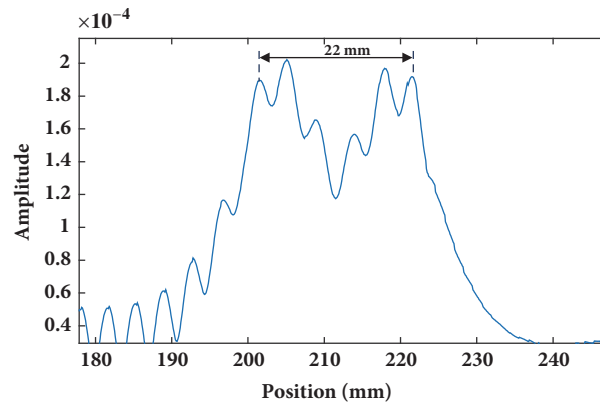


FIGURE 19: Cut of $S(x, f)$ at the frequency 300 kHz.

is sensitive to the position and to the length of delamination; this makes it an effective tool to evaluate the delamination in orthotropic material. Besides, based on signal changes with the delamination edges, a localization method is proposed to estimate the position and the length of the delamination. The proposed method was validated based on previous experimental work.

These are the main results:

- (i) The estimation is accurate when the delamination length increases.
- (ii) The optimal position to evaluate the beginning and the length of delamination is between the actuator and the defect which corresponds to the pulse-echo method.

As perspective, we model the whole sandwich structure and we characterize the defect by reflection and transmission coefficients.

Data Availability

The data used to support the findings of this study are available from the corresponding author upon request.

Conflicts of Interest

The authors declare that there are no conflicts of interest regarding the publication of this paper.

Acknowledgments

The research and publication of this article were funded by FST, Settat. The authors would like to express their gratitude to Elhadji Barra Ndiaye, Ph.D., for his help in the model verification.

References

- [1] Z. Tian, L. Yu, and C. Leckey, "Delamination detection and quantification on laminated composite structures with Lamb waves and wavenumber analysis," *Journal of Intelligent Material Systems and Structures*, vol. 26, no. 13, pp. 1723–1738, 2015.
- [2] B. Feng, A. L. Ribeiro, and H. G. Ramos, "Interaction of lamb waves with the edges of a delamination in CFRP composites," in *Proceedings of the 2017 IEEE International Workshop on Metrology for AeroSpace (MetroAeroSpace)*, pp. 217–222, Padua, Italy, June 2017.
- [3] W. Chiu, L. Rose, and N. Nadarajah, "Scattering of the fundamental anti-symmetric lamb wave by a mid-plane edge delamination in a fiber-composite laminate," *Procedia Engineering*, vol. 188, pp. 317–324, 2017.
- [4] N. Guo and P. Cawley, "The interaction of Lamb waves with delaminations in composite laminates," *The Journal of the Acoustical Society of America*, vol. 94, no. 4, pp. 2240–2246, 1993.
- [5] N. Nadarajah, B. S. Vien, and W. K. Chiu, "Computational study of the A0 scattered field due to an edge delamination," *Journal of Mechanics Engineering and Automation*, vol. 5, no. 4, 2015.
- [6] T. Hayashi and K. Kawashima, "Multiple reflections of Lamb waves at a delamination," *Ultrasonics*, vol. 40, no. 1-8, pp. 193–197, 2002.
- [7] C.-T. Ng and M. Veidt, "Scattering of the fundamental anti-symmetric Lamb wave at delaminations in composite laminates," *The Journal of the Acoustical Society of America*, vol. 129, no. 3, pp. 1288–1296, 2011.
- [8] B. Yang, F.-Z. Xuan, S. Chen, S. Zhou, Y. Gao, and B. Xiao, "Damage localization and identification in WGF/epoxy composite laminates by using Lamb waves: Experiment and simulation," *Composite Structures*, vol. 165, pp. 138–147, 2017.
- [9] S. Mustapha and L. Ye, "Propagation behaviour of guided waves in tapered sandwich structures and debonding identification using time reversal," *Wave Motion*, vol. 57, pp. 154–170, 2015.
- [10] C. T. Ng, M. Veidt, L. R. F. Rose, and C. H. Wang, "Analytical and finite element prediction of Lamb wave scattering at delaminations in quasi-isotropic composite laminates," *Journal of Sound and Vibration*, vol. 331, no. 22, pp. 4870–4883, 2012.
- [11] M. Veidt and C.-T. Ng, "Influence of stacking sequence on scattering characteristics of the fundamental anti-symmetric Lamb wave at through holes in composite laminates," *The Journal of the Acoustical Society of America*, vol. 129, no. 3, pp. 1280–1287, 2011.
- [12] A. De Luca, Z. Sharif-Khodaie, M. H. Aliabadi, and F. Caputo, "Numerical Simulation of the Lamb Wave Propagation in Impacted CFRP Laminate," *Procedia Engineering*, vol. 167, pp. 109–115, 2016.

- [13] C. Yang, L. Ye, Z. Su, and M. Bannister, "Some aspects of numerical simulation for Lamb wave propagation in composite laminates," *Composite Structures*, vol. 75, no. 1-4, pp. 267–275, 2006.
- [14] E. B. Ndiaye, "Contrôle santé de structures sandwichs composites, caractérisation et évaluation non destructives de l'adhésion et du vieillissement Simulations par éléments finis et expérimentation par mesure d'impédance et par ultrasons multiéléments , Université du Havre," Université du Havre, École Doctorale S.P.M.I.I, 2014.
- [15] DISPERSE user's manual, version 2.0.11, 2001.
- [16] D. Alleyne and P. Cawley, "A two-dimensional Fourier transform method for the measurement of propagating multimode signals," *The Journal of the Acoustical Society of America*, vol. 89, no. 3, pp. 1159–1168, 1991.
- [17] K.-H. Ip and Y.-W. Mai, "Delamination detection in smart composite beams using Lamb waves," *Smart Materials and Structures*, vol. 13, no. 3, pp. 544–551, 2004.
- [18] R. Basri and W. K. Chiu, "Numerical analysis on the interaction of guided Lamb waves with a local elastic stiffness reduction in quasi-isotropic composite plate structures," *Composite Structures*, vol. 66, no. 1-4, pp. 87–99, 2004.
- [19] R. S. Panda, "Lamb wave interactions with delaminations in composite laminates using air-coupled ultrasonic visualization," in *Proceedings of the 14th Asia-Pacific Conference on Non-Destructive Testing*, 2013.
- [20] C. Ramadas, K. Balasubramaniam, M. Joshi, and C. V. Krishnamurthy, "Interaction of the primary anti-symmetric Lamb mode (A_0) with symmetric delaminations: Numerical and experimental studies," *Smart Materials and Structures*, vol. 18, no. 8, 2009.
- [21] R. Soleimanpour and C.-T. Ng, "Mode conversion and scattering analysis of guided waves at delaminations in laminated composite beams," *Structural Monitoring and Maintenance*, vol. 2, no. 3, pp. 213–236, 2015.
- [22] P. Gudimetla and A. Kharidi, "Simulation of delaminations in composite laminates," in *Proceedings of the International Conference on Precision, Meso, Micro and Nano Engineering*, pp. 11-12, 2009.
- [23] E. B. Ndiaye and H. Duflo, "Non destructive testing of sandwich composites: adhesion defects evaluation; experimental and finite element method simulation comparison," in *Proceedings of the Acoustics 2012 Nantes Conference*, 2012.
- [24] N. Bourasseau, E. Moulin, C. Delebarre, and P. Bonniau, "Radome health monitoring with Lamb waves: Experimental approach," *NDT & E International*, vol. 33, no. 6, pp. 393–400, 2000.
- [25] K. Diamanti, J. M. Hodgkinson, and C. Soutis, "Application of a lamb wave technique for the non destructive inspection of composite structures," in *Proceedings of the 1th European Conference on Composite Materials*, Rhodes, Greece, 2004.
- [26] G. Bonnet, "Au-delà d'une vitesse de groupe: vitesse de phase et vitesse de signal. Première partie: l'opérateur vitesse de groupe en l'absence d'affaiblissement," *Annales des Télécommunications*, vol. 38, no. 9-10, pp. 1–22, 1983.
- [27] G. Bonnet, "Au-delà d'une vitesse de groupe: vitesse de phase et vitesse de signal. Première partie: déformation de l'amplitude et influence de l'affaiblissement," *Annales des Télécommunications*, vol. 38, no. 11-12, pp. 1–17, 1983.

